

Potential Contrast – A New Image Quality Measure

Arie Shaus, Shira Faigenbaum-Golovin, Barak Sober, Eli Turkel, Eli Piasezky; Tel Aviv University; Tel Aviv, Israel

Abstract

This paper suggests a new quality measure of an image, pertaining to its contrast. Several contrast measures exist in the current research. However, due to the abundance of Image Processing software solutions, the perceived (or measured) image contrast can be misleading, as the contrast may be significantly enhanced by applying grayscale transformations. Therefore, the real challenge, which was not dealt with in the previous literature, is measuring the contrast of an image taking into account all possible grayscale transformations, leading to the best “potential” contrast. Hence, we suggest an alternative “Potential Contrast” measure, based on sampled populations of foreground and background pixels (e.g. scribbles or saliency-based criteria). An exact and efficient implementation of this measure is found analytically. The new methodology is tested and is shown to be invariant to invertible grayscale transformations.

Introduction

Establishing the contrast of an image is a well-studied problem in the fields of Optics and Image Processing. Several measures have been proposed, for that purpose, in the past. Among these are the contrast measures of Weber [1], Michelson [1, 2], root-mean-square contrast and its enhancements [3,4], CMI [5-8], as well as measures based on frequency domain analysis [1,9], wavelet transforms [9,10] and edge detection [11,12].

However, the problem is complicated by the immense set of transformations which can be applied to the image, potentially improving its contrast. Given a proliferation of the available Image Processing software solutions, applying such enhancements is almost indispensable. Therefore, the real challenge, which was not dealt with in the previous literature, is *measuring the contrast of an image taking into account all its possible transformations*. In this article, we will limit ourselves to the wide range of *grayscale transformations*.

Prior Art

Various algorithms were designed to give an objective contrast measure that correlates with human assessment. In what follows, we consider grayscale images of the form $I : [1, L] \times [1, M] \rightarrow [0, 255]$ (unless stated otherwise, throughout the article, the intervals are assumed to be subsets of integers). We review several popular contrast measures, stating their relative shortcomings.

A simple way of measuring a bi-population image contrast is calculating the ratio between foreground and background:

$$\text{SimpleContrast} := \mu_B / \mu_F \quad (1)$$

where μ_B and μ_F are the averages of the sampled background and foreground luminance values, respectively.

A more commonly used measure (closely related to *SimpleContrast*) is Weber's contrast ratio [1] defined as:

$$\text{Weber} := \frac{\mu_B - \mu_F}{\mu_B} = 1 - \frac{1}{\text{SimpleContrast}} \quad (2)$$

Another prominent contrast ratio measure is given by Michelson [1, 2]:

$$\text{Michelson}_{\min \max} := \frac{I_{\max} - I_{\min}}{I_{\max} + I_{\min}} \quad (3)$$

where I_{\max} and I_{\min} are the maximal and minimal luminance values of the entire image, respectively. This definition can be adapted to the case of bi-population images as follows:

$$\text{Michelson} := \frac{\mu_B - \mu_F}{\mu_B + \mu_F} \quad (4)$$

The ratios (1), (2) and (4) result in different values for a single image. Nevertheless, given a set of images, the *ordering* based upon them will be identical. This can be verified via algebraic manipulations.

A different statistical approach is the root-mean-square contrast [3]:

$$\text{RMS} := \left[\frac{1}{LM} \sum_{l=1..L, m=1..M} (I(l, m) - \bar{I})^2 \right]^{1/2} \quad (5)$$

where $I(l, m) \in [0, 1]$ is a normalized gray level and

$\bar{I} = \frac{1}{LM} \sum_{l=1..L, m=1..M} I(l, m)$. Another, closely related statistical-based

measure is suggested by [4].

A very simple, yet valuable contrast measure, developed and utilized in [5-8] for the purpose of historical document analysis, is the CMI index:

$$\text{CMI} := \mu_B - \mu_F \quad (6)$$

This measure will play an important role in the current paper.

Some additional approaches are based on frequency domain analysis (e.g. [1,9]), wavelet transforms (e.g. [9,10]) and edge detection (e.g. [11,12], that also deal with contrast improvements).

Popular image enhancements bear the potential of improving the image quality. These include brightening and darkening, histogram stretching and equalization - all performed by grayscale transformations. Unfortunately, all of the above mentioned measures are affected, to some extent, by such transformations. For instance, the Weber and Michelson ratios are not invariant to grayscale shifts, the CMI is not invariant to grayscale rescalings, while all the measures are not invariant to histogram equalizations. This aspect is demonstrated in Fig. 1 and Table I. The RMS seems relatively stable with respect to most of the grayscale transformations. Unfortunately, although its definition represents the standard deviation of the image, which is an important statistic, it does not quantify the quality of separation between foreground and background.



Figure 1. Example of images undergoing grayscale transformations. (a) original image with sampled foreground (in red) and background (in blue). (b) the image after brightness change (+70) (c) the image after histogram rescaling (x1.3) (d) the image after histogram equalization.

Table I: Contrast Measures Comparison Based On Fig. 1

Image	Weber	Michelson	RMS	CMI	
(a) Original	I	0.535	0.365	1.42×10^{-4}	90.6
(b) Brightened	$I + 70$	0.378	0.233	1.42×10^{-4}	90.6
(c) Rescaled	$I \cdot 1.3$	0.536	0.366	1.43×10^{-4}	117.7
(d) Equalized	$eq(I)$	0.33	0.197	1.27×10^{-4}	72.1

Problem Setting

Given a contrast measure m , and an image I , the task is finding a grayscale transformations $g \in G := \{[0, 255] \rightarrow [0, 255]\}$ maximizing $m(g \circ I)$. At first glance, this may seem as a computational-intensive undertaking, since the set of transformations of a given image is immense ($2^{2^{B+\log_2 B}}$ for images of bit-depth B). The main contribution of this paper is a constructive procedure for finding the optimal transformation g *analytically*, for a particular measure m . This would lead to a definition of a new, “potential” contrast measure, possessing the following properties:

1. Quantifying the difference between foreground and background pixels (i.e. the measure is a meaningful one).
2. Images will be judged according to their **potential** for improvements via **all possible** grayscale transformations (i.e. the measure is “aware” of the possibility to perform image enhancements such as brightening, rescaling and equalizing its grayscale levels).
3. In particular, the measure ought to be invariant to **invertible** grayscale transformations (as the inherent information of the image is preserved and the potential for image improvement after such transformation is maintained).

Measure Definition

Definition of Potential Contrast

In order to deal with this problem analytically, we restrict ourselves to the CMI measure defined in Eq. 6, $m = CMI$. Furthermore, we deal with a case of sampled histograms (“populations”) of foreground and background pixels, as is observed in Fig 1a. These are respectively denoted as $\{p_F(t)\}_{t=0}^{255}$ and $\{p_B(t)\}_{t=0}^{255}$ (satisfying $0 \leq p_F(t) \leq 1$, $0 \leq p_B(t) \leq 1$ and $\sum_{t=0}^{255} p_F(t) = \sum_{t=0}^{255} p_B(t) = 1$).

We begin with finding the maximal $CMI(g \circ I)$ for an image I , with the wealth of optional grayscale transformations g , proceeding with the definition of a new measure.

Proposition I (optimality):

For a given image I , with sampled populations $\{p_F(t)\}_{t=0}^{255}$ and $\{p_B(t)\}_{t=0}^{255}$ (as denoted above), the optimal grayscale transformation with respect to the CMI measure is:

$$g_t^{opt}(t) := \arg \max_{g \in G} CMI(g \circ I) = \begin{cases} 0 & p_F(t) > p_B(t) \\ 255 & p_F(t) \leq p_B(t) \end{cases} \quad (7)$$

Proof:

$$\begin{aligned} CMI(g \circ I) &= \sum_{t=0}^{255} g(t)p_B(t) - \sum_{t=0}^{255} g(t)p_F(t) = \sum_{t=0}^{255} g(t)[p_B(t) - p_F(t)] \leq \\ &\leq \sum_{\substack{t=0 \\ p_B(t) \geq p_F(t)}}^{255} 255 \cdot [p_B(t) - p_F(t)] + \sum_{\substack{t=0 \\ p_B(t) < p_F(t)}}^{255} 0 \cdot [p_B(t) - p_F(t)] = \\ &= \sum_{t=0}^{255} g_t^{opt}(t)p_B(t) - \sum_{t=0}^{255} g_t^{opt}(t)p_F(t) = CMI(g_t^{opt} \circ I) \end{aligned}$$

Definition: The *Potential Contrast* (PC) of an image is:

$$PC(I) := CMI(g_t^{opt} \circ I) \quad (8)$$

Remarks:

1. Due to its nature, the PC measure reflects the innate image quality, not necessarily compatible with immediate human impression. Consider a pair of images created from the same source (Fig. 1a), one with added Gaussian noise (Fig. 2a), while the other brightened to some extent (Fig. 2b). Although the former may be viewed as more contrasted, in fact the latter has considerably higher Potential Contrast (PC=206.28 vs. PC=255.0). This is due to the fact that it possesses the same information as the original image, unlike the image with Gaussian noise.



Figure 2. An example of misleading naked eye: Two images stemming from the same source, with the same sampled populations (Fig. 1a). (a) added Gaussian noise of $\mu=0$, $\sigma=32$, $PC=206.28$ (b) narrowing the dynamic range and brightening ($pixel_value/4+200$), $PC=255.00$.

2. Foreground and background selection can be performed in numerous ways. These choices represent diverse, often incompatible, needs of human operators. For example, in Fig. 3, what are the expected foreground and background? Are they respectively the kettle and the chair? Or maybe the writing and the whiteboard?

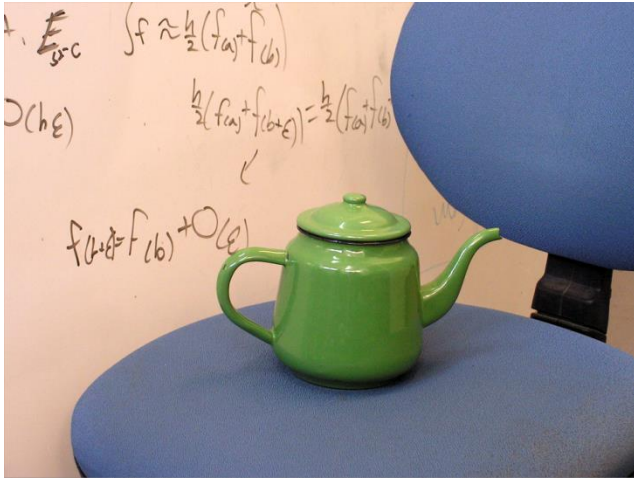


Figure 3. Example of ambiguous foreground and background. While it is possible that the kettle is the foreground and the chair is the background, writing as a foreground and whiteboard as a background is another viable option.

Therefore, in our view, no “ultimate” background and foreground selections encompassing all feasible tasks can be defined. This explains our preference for sampled foreground and background populations – the foreground and the background are in the eyes of the beholder. Nonetheless, a “naïve” suggestion for automatic foreground and background estimation is proposed below.

3. The CMI was chosen as a basis for the Potential Contrast definition due to the possibility of optimizing analytically the measure for all possible grayscale transformations. We did not succeed to similarly utilize other measures.

Measure Properties

Population separability: g_i^{opt} may be viewed as a function separating between foreground and background populations. This function serves as a *classifier*, denoted herein as *PC-binarization*. If the populations are separable by a certain threshold (e.g. distinct Gaussians), the function can be represented as:

$$g_i^{opt}(t) = \begin{cases} 0 & t \leq T \\ 255 & t > T \end{cases} \quad (9)$$

However, this is not the general case (which can be seen in Eq. 7). Fig. 4 provides an example of grayscale histogram not separable by thresholding, while easily classifiable by the PC framework.

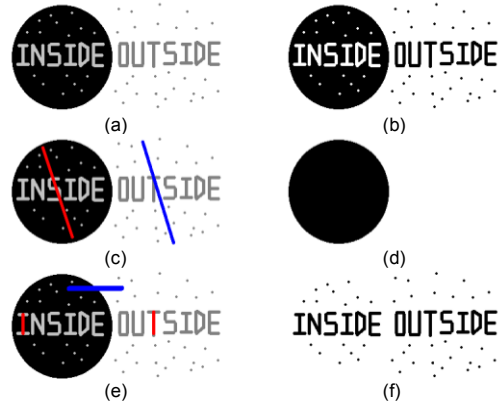


Figure 4. Example of foreground and background not separable by thresholding, while easily classifiable by the PC framework. (a) original grayscale image (circle=0, writing within the circle=195, writings outside the circle=127, other areas outside the circle=255), (b) example of thresholded image (c) circle and its content as foreground (in red) with the rest as background (in blue), (d) PC-binarization based on (c), (e) writing as foreground (in red) with the rest as background (in blue), (f) PC-binarization based on (e).

In fact, even a slight difference in gray levels between the two populations may suffice to achieve a reasonable separation, i.e. binarization. See an example of “challenging” contrast enhancement in Fig. 5, based on the RGB decomposition of the original image, with several resulting PC-binarizations.

Complexity: The calculation of foreground and background histograms is linear in the number of pixels ML , which tends to be small. The construction of g_i^{opt} is only dependent on the number of levels in the histogram. Therefore, for a grayscale image of 256 levels, the overall complexity is $O(ML + 256)$. Hence, the complexity is linear with respect to the number of pixels.

Equivalence to error estimation: $PC(I)$ can be viewed as a measure minimizing the rate of false positives (FP) and false negatives (FN) mistakes, i.e. confusing foreground for background and vice-versa. This follows from the fact that:

$$PC(I) = \sum_{t=0}^{255} 255 \cdot [p_B(t) - p_F(t)] = 255 - \sum_{t=0}^{255} 255 \cdot p_B(t) - \sum_{t=0}^{255} 255 \cdot p_F(t) = 255 \cdot (1 - FP - FN)$$

In the case of perfect separability of populations, the PC would be maximal, i.e. 255. Note: this is the case in Figs. 2b, 4c and 4e.

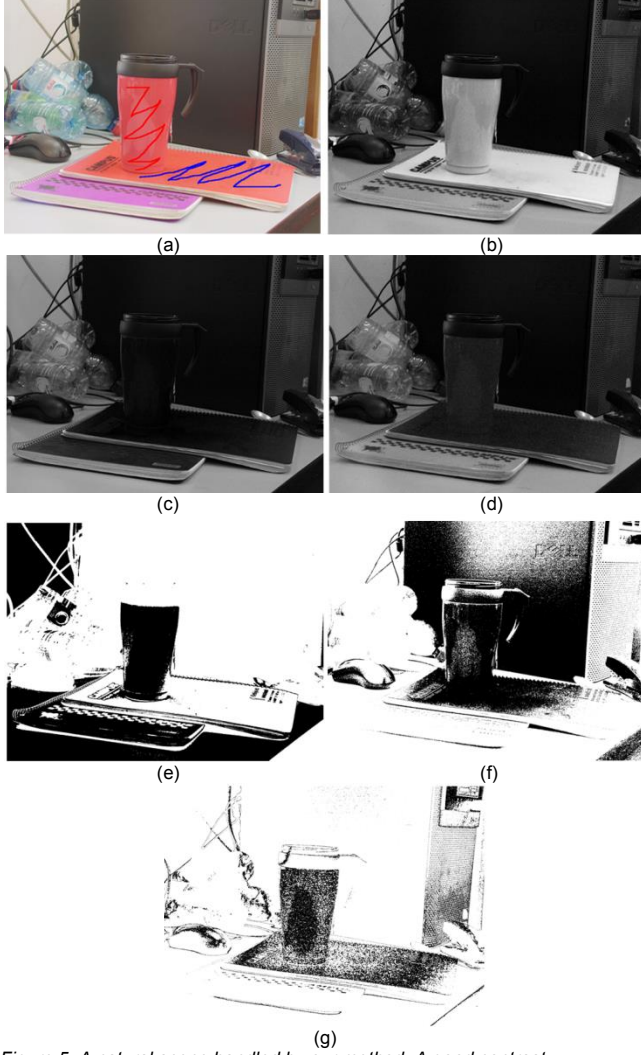


Figure 5. A natural scene handled by our method. A good contrast enhancement is achieved despite the similarity in foreground and background shade. (a) RGB image of the scene with manual selection of foreground in red and background in blue; R (b), G (c) and B (d) channels, with respective PC values of 244.8, 67.6 and 61.2; the PC-binarizations for R (e), G (f) and B (g).

Symmetry between foreground and background: The last property proves that if we replace the foreground sampled histogram with the background sampled histogram and vice-versa, the result of the PC measure is the same. On the other hand, the respective PC-binarizations would be each other's negatives.

Proposition II (invariance with respect to invertible g):

Given an image I , and an invertible $g \in G$, $PC(I) = PC(g \circ I)$.

Proof:

g is invertible, therefore $\exists g^{-1} \in G$. $g^{-1} \circ g = \text{identity}$. Thus:

$$PC(I) = CMI(g_I^{opt} \circ I) = CMI(g_I^{opt} \circ g^{-1} \circ g \circ I)$$

Denoting: $h := g_I^{opt} \circ g^{-1}$ and $J := g \circ I$:

$$PC(I) = CMI(h \circ J)$$

Assuming $h \neq g_J^{opt}$, then:

$$PC(I) = CMI(h \circ J) < PC(J) = CMI(g_J^{opt} \circ J) = CMI(g_J^{opt} \circ g \circ I)$$

A contradiction to the optimality of g_I^{opt} .

Therefore, $PC(I) = PC(g \circ I)$. ■

Remark: This defines the following equivalence relation between two images:

$$I_1 \sim I_2 \Leftrightarrow \exists g \text{ invertible s.t. } I_1 = g \circ I_2$$

The invariance property of the PC, with respect to the images of Fig. 1, is demonstrated in Table II. This supplements and contrasts with the results in Table I.

Table II: PC measure based on Fig. 1

Image		PC
(a) Original	I	255.00
(b) Bright	$I + 70$	255.00
(c) Rescaled	$I \cdot 1.3$	255.00
(d) Equalized	$eq(I)$	254.98

Automated Foreground/Background Selection

As stated above, the foreground and background selection largely depends on the specific task and usage scenario. Nevertheless, one generic approach would be to utilize one of the existing saliency estimation techniques. Fortunately, a useful and enlightening comparison of the leading saliency methods is presented in [13]. Surprisingly, among the “leading” saliency methods is a simple saliency map dependent on the distance of each pixel from the center of the image. In this estimation, 255 (the most salient value) is assigned to the central pixels, while 0 (the least salient value) is assigned to its corners. The empirical success of this unsophisticated technique probably has to do with either conscious or unconscious preference of human photographers for images centered on the object of their interest.

Despite Bylinskii *et al.*'s [13] claim of using a Gaussian model in this estimation, a reverse-engineering of their saliency image reveals a replacement of the Gaussian with a second-order polynomial approximation. In particular, given an image $I(x, y) : [1, L] \times [1, M] \rightarrow [0, 255]$, the saliency (i.e. foreground) map $S(x, y) : [1, L] \times [1, M] \rightarrow [0, 255]$ is constructed via the following formula:

$$S(x, y) = 255 \cdot \left(1 - \frac{1}{2} \left(\left(\frac{x - L/2}{L/2} \right)^2 + \left(\frac{y - M/2}{M/2} \right)^2 \right) \right) \quad (10)$$

It is easy to see that this formula satisfies $S(0, 0) = S(L, 0) = S(0, M) = S(L, M) = 0$, $S(L/2, M/2) = 255$, as well as $0 \leq S(x, y) \leq 255$. Examples of such a saliency map used for the foreground, as well as its complimentary $255 - S(x, y)$ used for the background, can be seen in Fig. 6.

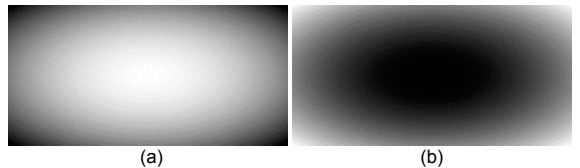


Figure 6. An example of automatically created saliency-based foreground (a) and background (b) maps.

Naturally, utilization of such continuous maps comes with the small price of adapting the measures. Indeed, apart from RMS (which does not rely on either the foreground or the background),

all the measures utilize “crisp” definitions of the foreground and background populations. Fortunately, the measures’ definitions can be easily adapted for a “fuzzy” case, in which each pixel belongs to both the foreground and the background with a certain probability (in fact $S(x,y)/255$ for foreground and $(255 - S(x,y))/255$ for background). E.g., μ_F and μ_B now become weighted means, while $\{p_F(t)\}_{t=0}^{255}$ and $\{p_B(t)\}_{t=0}^{255}$ represent weighted histograms over the entire image – maintaining the properties of the PC measure.

Experimental Results

The purpose of the following experiments is to empirically validate the behavior of the various contrast metrics including the Potential Contrast, with an emphasis on their invariant properties. The experiment consisted of the following steps:

1. The input for the experiments were images belonging to the popular GRAZ-02 data set, containing natural images [14]. This included all images under the categories “bike”, “car” and “person”, which possessed a ground truth. With 300 files in each category, this resulted in 900 files.
2. If needed, each image was converted to grayscale by averaging its channels. The histogram of the result was rescaled between 25 and 230 (maintaining the full dynamic range in transformations applied in the next step). This rescaled image is denoted herein as “initial” image.
3. Various gray-level transformations were applied to the “initial” image. This resulted in 6 additional images for each “initial” image. The transformations in use were: negative of an image, addition of 25, subtraction of 25, multiplication by 1.1, histogram stretching (from 0 to 255), and histogram equalization (from 0 to 255). In total, further $900 \times 6 = 5400$ images were obtained.
4. Five contrast measures (Weber, Michelson, RMS, CMI and PC) were applied on all the images (“initial” and transformations). The calculation used either marked background and foreground (utilizing ground truths from [14]), or an automated foreground and background selection scheme, as described above (the results for these two types of experiments are presented separately below).
5. For a given measure, the result for each transformation was divided by the result of the “initial” image, in order to obtain a “ratio of change” (e.g., if a given measure results in 2.718 on “initial” image, and in 3.14 on a transformed one, the division produces a ratio of 1.1557).
6. Ratios within the range of $[0.99, 1.01]$ were marked as indicating “invariance” of the measure with respect to a particular transformation, while others were counted as “non-invariant” outcomes. The percentage of the “invariant” ratios was calculated.

Experiment Results for Manual Foreground and Background Selection

The results in Table III were achieved by using existing ground truths, marking foreground and background.

Table III: Manual foreground and background selection: Ratios between the measures of transformed images with respect to the “initial” image (predicted invariance marked in red).

Transformation	Statistics	Weber	Michelson	RMS	CMI	PC
Negative	Minimum	-2.8741	-1.7535	1	-1	1
	Maximum	-0.1468	-0.1842	1	-1	1
	Average	-0.8913	-0.7291	1	-1	1
	Invariance %	0.0%	0.0%	100.0%	0.0%	100.0%
+25	Minimum	0.5663	0.6134	1	1	1
	Maximum	0.8833	0.8666	1	1	1
	Average	0.8167	0.8032	1	1	1
	Invariance %	0.0%	0.0%	100.0%	100.0%	100.0%
-25	Minimum	1.1523	1.1820	1	1	1
	Maximum	4.2715	2.7046	1	1	1
	Average	1.3132	1.3391	1	1	1
	Invariance %	0.0%	0.0%	100.0%	100.0%	100.0%
x1.1	Minimum	1	1	1	1.1	1
	Maximum	1	1	1	1.1	1
	Average	1	1	1	1.1	1
	Invariance %	100.0%	100.0%	100.0%	0.0%	100.0%
Histogram stretching	Minimum	1.1523	1.1820	1	1.2439	1
	Maximum	4.2715	2.7046	1	1.2439	1
	Average	1.3132	1.3391	1	1.2439	1
	Invariance %	0.0%	0.0%	100.0%	0.0%	100.0%
Histogram equalization	Minimum	-99.4991	-102.5043	0.7581	-100.0948	0.9727
	Maximum	20.0625	19.6348	4.5870	19.2820	1.0000
	Average	1.3029	1.4134	1.5294	1.5560	0.9983
	Invariance %	0.7%	0.8%	1.1%	0.6%	98.7%

As expected, the most invariant and well-behaving metrics are RMS and Potential Contrast. However, only the latter holds an almost-perfect invariance on histogram equalization transformation, whose non-linearity breaks the RMS record.

Experiment Results for Automated Foreground and Background Estimation

The results, which can be seen in Table IV, were achieved by using automated foreground and background estimation.

Transformation	Statistics	Weber	Michelson	RMS	CMI	PC
Negative	Minimum	-2.0264	-1.7467	1	-1	1
	Maximum	-0.1561	-0.1679	1	-1	1
	Average	-0.8588	-0.8406	1	-1	1
	Invariance %	0.0%	0.0%	100.0%	0.0%	100.0%
+25	Minimum	0.5794	0.5945	1	1	1
	Maximum	0.8723	0.8664	1	1	1
	Average	0.8143	0.8138	1	1	1
	Invariance %	0.0%	0.0%	100.0%	100.0%	100.0%
-25	Minimum	1.1715	1.1823	1	1	1
	Maximum	3.6483	3.1459	1	1	1
	Average	1.3161	1.3144	1	1	1
	Invariance %	0.0%	0.0%	100.0%	100.0%	100.0%
x1.1	Minimum	0.2481	0.2481	0.9993	0.2730	1
	Maximum	1.0399	1.0399	1.0039	1.1443	1
	Average	0.9980	0.9980	1.0023	1.0983	1
	Invariance %	96.7%	96.7%	100.0%	0.0%	100.0%
Histogram stretching	Minimum	0.5342	0.5342	0.9993	0.5426	1
	Maximum	3.6398	3.1516	1.0033	3.0089	1
	Average	1.3175	1.3158	1.0001	1.2452	1
	Invariance %	0.0%	0.0%	100.0%	0.0%	100.0%
Histogram equalization	Minimum	-2977.7504	-2740.1799	0.7597	-2664.9400	0.9718
	Maximum	351.1975	336.0259	4.5821	326.7109	1
	Average	-0.8685	-0.6326	1.5308	-0.3027	0.9983
	Invariance %	0.1%	0.1%	1.0%	0.4%	99.1%

Since this experiment is based on an estimated foreground and background, which may be quite far from a clear-cut partition of an image, the outcomes are expected to be less numerically stable. Indeed, the results for many transformations are much more spread-out. Nevertheless, yet again, the challenging histogram equalization provides a clear winner. In fact, it doesn’t seem that the stability of Potential Contrast was significantly hampered by the inaccuracy and fuzziness in the foreground and background selection.

Additional Usage and Results

The PC measure received extensive real-world usage, applied on multispectral imagery of large corpora of ancient inscriptions. The first problem included a selection of optimal wavelengths for multispectral imagery of Second Temple Period Dead Sea Scrolls [15]. See Fig. 7a for an example of such a scroll, with a correct channel automatically selected and binarized in Fig. 7b.

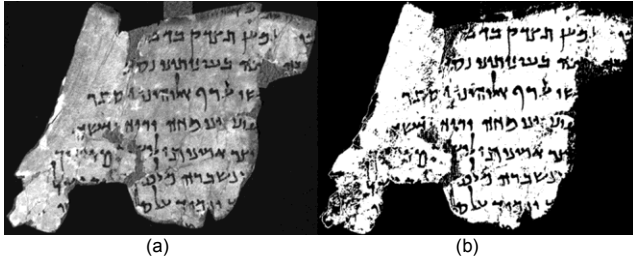


Figure 7. Section of Dead Sea scroll #124, fragment 001 [15]. (a) Image of a scroll (b) PC-binarization of (a).

Another test for our technique had to do with First Temple Period Hebrew, as well as Late Bronze Hieratic (cursive Egyptian) ink-on-clay inscriptions. These were unearthed during the excavations of Horvat Radum and Horvat Uza (e.g. Figs. 8, 9) [16,17], Tel Malhata [18,19], Qubur el-Walaydah (e.g. Fig. 10) [20] and Jerusalem [21]. The difficult and noisy medium of the ink written on pottery sherds presented a good opportunity to test the new methodology. Again, our task was to automatically select the “potentially” most contrasted image out of a spectral cube, in order to allow further analysis by human scholars. See Figs. 8-10 for examples of ostraca handled by our method, in order to find an optimal imaging wavelength. An elaboration of our experiments pertaining to this particular use case appears in [22].

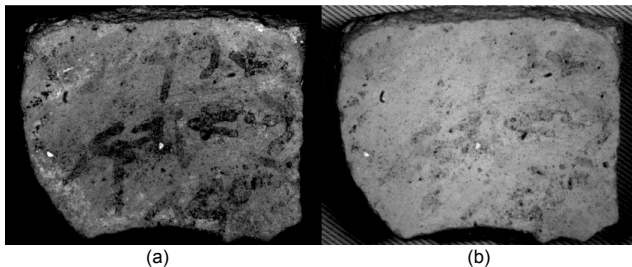


Figure 8. Images of Horvat Radum ostracon No. 1 [16,17]. (a) optimal image at $\lambda=620$ nm, selected by our method (b) sub-optimal image at $\lambda=950$ nm.

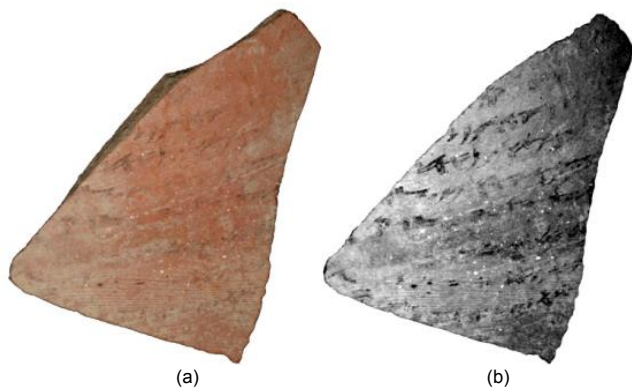


Figure 9. Images of ostracon No. 3 from Horvat Uza [16,17]. (a) RGB image (b) multispectral image taken at $\lambda=660$ nm, selected by our method.

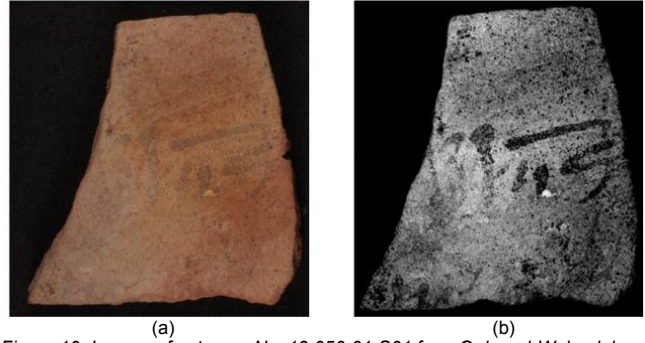


Figure 10. Images of ostracon No. 13.056-01-S01 from Qubur el-Walaydah [20]. (a) RGB image, (b) multispectral image taken at $\lambda=690$ nm, selected by our method.

Summary

This paper presents a new approach for contrast estimation. Using available Image Processing software, an image can undergo various grayscale transformations, often improving its contrast. The common contrast evaluation methods, surveyed in this article, do not take this possibility into account.

Our Potential Contrast measure encompasses an analytic solution to the problem of finding the most contrasting grayscale transformation. The properties of the Potential Contrast were tested and compared to other measures on a large data set of 900 images, in two scenarios of foreground and background selection. The results indicate the invariance and the stability of the measure with respect to various gray-scale transformations.

Acknowledgments

The research reported here received initial funding from the Israel Science Foundation – F.I.R.S.T. (Bikura) Individual Grant no. 644/08, as well as the Israel Science Foundation Grant no. 1457/13. The research was also funded by the European Research Council under the European Community's Seventh Framework Programme (FP7/2007-2013)/ERC grant agreement no. 229418, and by an Early Israel grant (New Horizons project), Tel Aviv University. This study was also supported by a generous donation from Mr. Jacques Chahine, made through the French Friends of Tel Aviv University. Arie Shaus is grateful to the Azrieli Foundation for the award of an Azrieli Fellowship. This research is in debt to the late Prof. Itzhaq Beit-Arieh. We wish to thank Ms. Liora Freud, Dr. Shirly Ben-Dor Evian, Ms. Tamar Lavee, Prof. Israel Finkelstein, Prof. David Levin and Prof. Murray Moinester. Ostraca images: courtesy of the Institute of Archaeology, Tel Aviv University (photographer: Michael Cordonsky) and the Israel Antiques Authority. Full spectrum color images of the Dead Sea Scrolls courtesy of the Israel Antiques Authority (photographer: Shai Halevi) [15].

References

- [1] E. Peli, “Contrast in Complex Images,” J. Opt. Soc. Am. A, vol. 7, pp. 2032-2040, 1990.
- [2] A. A. Michelson, Studies in Optics, University of Chicago Press, 1927.
- [3] M. Pavel, G. Sperling, T. Riedl, A. Vanderbeek, “Limits of Visual Communication: The Effect of Signal-to-noise Ratio Tin the Intelligibility of American Sign Language,” J. Opt. Soc. Am. A, vol. 4, pp. 2355-2365, 1987.

- [4] A. Shio, "An Automatic Thresholding Algorithm Based on an Illumination-independent Contrast Measure," Proc. IEEE Computer Society Conference on Computer Vision and Pattern Recognition - CVPR 1989, pp. 632-637, 1989.
- [5] A. Shaus, E. Turkel, and E. Piasezky, "Quality Evaluation of Facsimiles of Hebrew First Temple Period Inscriptions," Proc. 10th IAPR International Workshop on Document Analysis Systems - DAS 2012, pp. 170-174, 2012.
- [6] A. Shaus, E. Turkel, and E. Piasezky, "Binarization of First Temple Period Inscriptions - Performance of Existing Algorithms and a new Registration Based Scheme," Proc. 13th International Conference on Frontiers in Handwriting Recognition - ICFHR 2012, pp. 641-646, 2012.
- [7] A. Shaus, I. Finkelstein, and E. Piasezky, "Avoiding the Eye of the Beholder: Automated Ostraca Facsimile Evaluation," *Maarav*, vol. 17, no. 1, pp. 7-20, 2010.
- [8] S. Faigenbaum-Golovin, A. Shaus, B. Sober, D. Levin, N. Naaman, B. Sass, E. Turkel, E. Piasezky, and I. Finkelstein, "Algorithmic Handwriting Analysis of Judah's Military Correspondence Sheds Light on Composition of Biblical Texts," Proceedings of the National Academy of Sciences, vol. 113, no. 17, pp. 4664-4669, 2016.
- [9] X. Li, D. Tao, X. Gao, W. Lu, "A Natural Image Quality Evaluation Metric," *Signal Process.*, vol. 89, no. 4, pp. 548-555, 2009.
- [10] Y. K. Lai, C. C. J. Kuo, "A Haar Wavelet Approach to Compressed Image Quality Measurement," *J. Visual Communication and Image Representation*, vol. 11, no. 1, pp. 17-40, 2000.
- [11] J. G. Leu, "Image Contrast Enhancement Based on the Intensities of Edge Pixels," *CVGIP: Graphical Models and Image Processing*, vol. 54, no. 6, pp. 497-506, 1992.
- [12] A. I. Négrate, A. Beghdadi, H. Dupoisot, "An Image Enhancement Technique and its Evaluation Through Bimodality Analysis," *CVGIP: Graphical Models and Image Processing*, vol. 54, no. 1, pp. 13-22, 1992.
- [13] Z. Bylinskii, T. Judd, A. Borji, L. Itti, F. Durand, A. Oliva, and A. Torralba, "MIT Saliency Benchmark" website, <http://saliency.mit.edu/>, accessed July 2016.
- [14] A. Opelt, A. Pinz, M. Fussenegger, and P. Auer, "Generic Object Recognition with Boosting", *IEEE Trans. on Pattern Analysis and Machine Intelligence*, vol. 28, no. 3, 416-431 (2006); http://www.emt.tugraz.at/~pinz/data/GRAZ_02, accessed July 2016.
- [15] Dead Sea Scrolls Digital Project, the Israel Museum, Jerusalem website, <http://dss.collections.imj.org.il>, accessed July 2016.
- [16] I. Beit-Arieh, Horvat 'Uza and Horvat Radum: Two Fortresses in the Biblical Negev, Tel Aviv: Emery and Claire Yass Publications in Archaeology, 2007.
- [17] B. Sober, S. Faigenbaum, I. Beit-Arieh, I. Finkelstein, M. Moinester, E. Piasezky, A. Shaus, "Enhancement of Ostraca Reading: Three Test Cases of Multispectral Imaging," *Palestine Exploration Quarterly*, vol. 146, no. 3, pp. 185-197, 2014.
- [18] I. Beit-Arieh and L. Freud, *Tel Malhata: A Central City in the Biblical Negev, Volume I*, Tel Aviv: Emery and Claire Yass Publications in Archaeology, 2015.
- [19] S. Faigenbaum, B. Sober, M. Moinester, E. Piasezky, and G. Bearman, "Multispectral Imaging of Tel Malhata Ostraca," In: I. Beit-Arieh, L. Freud, eds. *Tel Malhata: A Central City in the Biblical Negev, Volume I*. Tel Aviv: Emery and Claire Yass Publications in Archaeology, pp. 510-513, 2015.
- [20] S. Faigenbaum, B. Sober, I. Finkelstein, M. Moinester, E. Piasezky, A. Shaus, M. Cordonsky. "Multispectral Imaging of two Hieratic Inscriptions from Qubur el-Walaydah," *Ägypten und Levante*, vol. XXIV, pp. 349-53, 2014.
- [21] S. Faigenbaum-Golovin, C.A. Rollston, E. Piasezky, B. Sober, I. Finkelstein. "The Ophel (Jerusalem) Ostracon in Light of New Multispectral Images," *Semitica* vol. 57, pp. 113-37, 2015.
- [22] Faigenbaum, S., Sober, B., Shaus, A., Moinester, M., Piasezky, E., Bearman, G., Cordonsky, M., Finkelstein, I. "Multispectral Images of Ostraca: Acquisition and Analysis," *J. of Archaeological Science*, vol. 39, no. 12, pp. 3581-3590, 2012.

Author Biography

Arie Shaus is an alumnus of Adi Lautman Interdisciplinary Program for Outstanding Students. He received his B.Sc. in Mathematics (summa cum laude) in 2006, an M.Sc. in Applied Mathematics (cum laude) in 2011, and a B.A. in Archaeology (summa cum laude) in 2015, all from Tel Aviv University. Currently he is working on his Applied Mathematics Ph.D. thesis. His interests include image processing, machine learning, Biblical archaeology and Hebrew epigraphy.

Shira Faigenbaum-Golovin received her B.Sc. degree in Mathematics and Computer Science from Tel Aviv University, Israel, in 2006, and her M.Sc. in Applied Mathematics from Tel Aviv University in 2014. Her thesis topic was "Anisotropic Moving Least Squares". Currently, she is a PhD student in Applied Mathematics in Tel Aviv University. Her research interests include scattered data function approximation, machine learning, image processing of historical documents, author identification, multispectral image acquisition techniques, and Hebrew epigraphy.

Barak Sober received his B.Sc. degree in Mathematics and Philosophy from Tel Aviv University, Israel, in 2006. He received his M.Sc. in Applied Mathematics (summa cum laude) on the topic of "Handwritten Character Stroke Reconstruction" in 2013. He is currently pursuing his PhD in Applied Mathematics on the topic of "Approximation of Manifolds from Scattered Data". His interests include approximation theory, machine learning, image processing and archaeology.

Eli Turkel received the B.A. degree from Yeshiva University in 1965, and the M.S. and Ph.D. degrees from the Courant Institute, New York University, in 1967 and 1970. He is a professor emeritus in Mathematics at Tel Aviv University. His research interests include numerical analysis, inverse problems and image processing. He is listed as a highly cited author by the ISI Web of Knowledge. He is an associate editor of the Journal of Computational Physics.

Eli Piasezky received his B.Sc., M.Sc. and Ph.D. in Physics (respectively 1974, 1978, 1981), as well as B.A. in Archaeology (1999) from Tel Aviv University. From 1987, he is a Professor of Physics with the Sackler School of Physics and Astronomy, Tel Aviv University. His research interests are nuclear particle physics, radio-carbon dating and Iron Age inscriptions.